Int. J. Electrochem. Sci., 15**(2020)** 9759 – 9768, doi: 10.20964/2020.10.59

International Journal of
ELECTROCHEMICAL
SCIENCE
www.electrochemsci.org

Short Communication

Electrosynthesis of Iron-based ZrC Nanocomposite Powder in Molten Salt

Hongxia Liu[1,*],*Weihao Song*[1], *Qian Xu*[2,*],*Wen Ma*[1],*Yu Bai*[1]

[1] Inner Mongolia Key Laboratory of Thin Film and Coatings, School of Materials Science and Engineering, Inner Mongolia University of Technology, Hohhot 010051, Inner Mongolia, PR China
[2] State Key Laboratory of Advanced Special Steel, Shanghai University, Shanghai 200072, PR China.
[*]E-mail: pghx@163.com, qianxu@shu.edu.cn

Received: 30 June 2020/ *Accepted:* 5 August 2020 / *Published:* 31 August 2020

Iron-based ZrC nanocomposite powder is synthesized by using a simple electrochemical deoxidation process in $CaCl_2$-NaCl molten salt. Herein, the electrolysis is conducted at a constant potential using a graphite anode and a cost-effective $ZrSiO_4/Fe_2O_3$/carbon cathode. The reaction pathway of electrosynthesis is systematically investigated by examining the composition and microstructure of partially- and fully-reduced electrolytic products. The results reveal that the composition of Fe-based metallic phases in the final product can be controlled by adjusting the amount of Fe_2O_3 in the cathode precursor. Moreover, the formation of FeSi-ZrC composite is realized through the formation of calcium-containing intermediate phases, such as $CaZrO_3$, $Ca_xZr_{1-x}O_x$ and Ca_2SiO_4, oxycarbide phase, i.e., ZrC_xO_{1-x}, and Fe-Si intermetallics (Fe_3Si and Fe_5Si_3). The current study demonstrates the promise of electrochemical synthesis route for the fabrication of iron-based ZrC nanocomposites.

Keywords: Iron-based composite; ZrC; electrochemical synthesis; $ZrSiO_4$; molten salt

1. INTRODUCTION

Carbide-reinforced iron (Fe) matrix composites have garnered significant research attention due to their excellent wear properties and low cost[1]. TiC is widely used as reinforcement due to its high hardness, excellent wettability, superior chemical stability and desired compatibility with Fe-based matrix[2-4]. Similar to TiC, zirconium carbide (ZrC) possesses high melting point, excellent hardness and cubic structure[5-8]. Also, ZrC exhibits high-temperature tensile strength and creep strength as well as excellent room-temperature chemical stability[9]. It has been reported that the stability of ZrC is higher than TiC and the solubility of ZrC in Fe is lower than TiC[10]. Based on these unique characteristics, ZrC is being studied as reinforcement in Fe-matrix composites[11,12]. Besides, it has been demonstrated that the wear resistance and mechanical performance of Fe-matrix composites increase with the decrease of carbide particle size[1,13].

In general, the carbide-reinforced Fe matrix composites are prepared by the powder metallurgy route, which involves the introduction of carbide powder into the iron powder, rendering a composite with ultrafine carbides. However, the powder metallurgy route exhibits certain limitations[14]. Therefore, various other routes, such as melting and casting, carbothermic reduction, combustion synthesis and aluminothermic reduction, are proposed[2,14-17]. These routes involve the *in-situ* formation of carbide reinforcements, excluding the manufacturing and handling of the filler phase separately. However, the high working temperature (>1000 ℃) employed in these methods coarsens the carbide particles and leads to severe particle aggregation in the product. Hence, it is highly desired to develop a simple and relatively low-temperature technique to synthesize ZrC-reinforced Fe matrix nanocomposites. Recently, the electro-deoxidation process has been developed to directly synthesize different metals and alloys from corresponding solid oxides in molten salts[18-20]. Furthermore, different types of nano-crystalline carbides (e.g., TiC, NbC and HfC) and metal-carbide composites (e.g., Ti_5Si_3-TiC and Ni-TiC) can also be electrochemically synthesized by using oxide and carbon precursors at a relatively moderate temperature (750-900 °C)[21-25]. During the electrolysis process, metal oxides are electrochemically reduced for the extraction of metals/alloys and carbon powder is utilized for carbonization. However, the electrochemical synthesis of Fe-based ZrC nanocomposite has seldom been reported. Furthermore, one should note that the zirconium silicate or zircon ($ZrSiO_4$) represents an inexpensive source of zirconium. However, very few studies have utilized $ZrSiO_4$ to synthesize Fe-based ZrC cermet nanocomposites.

Herein, Fe-based ZrC nanocomposite powder is synthesized by using cost-effective precursors, such as zirconium silicate and Fe_2O_3, in the presence of carbon by a one-pot electrochemical process at 850 °C in $CaCl_2$-NaCl melt. The microstructure and phase composition of the Fe-based ZrC composites are examined by using SEM, TEM and XRD. The reaction pathway for molten salt electrosynthesis of FeSi-ZrC composites is also investigated by examining the variation in composition and microstructure of the cathode during electrolysis.

2. EXPERIMENTAL

$ZrSiO_4$ (Alfa Aesar; ZrO_2, 66%), Fe_2O_3 (China National Pharmaceutical Group Co., Ltd., China, Analytical reagent) and nanoscale carbon black (Tianjin No.3 Chemical Reagent Factory, China, Analytical reagent) powders were used as the cathode precursors. First, the stoichiometric amounts of $ZrSiO_4$, Fe_2O_3 and carbon black were ball-milled in ethanol for 4 h. Then, the slurry was vacuum dried for 5 h and the powder mixture was pressed into cylindrical pellets (Ø 15 × 1 mm) under a uniaxial pressure of 8 MPa. The pellets were sintered at 950 °C for 4 h under argon flow to obtain cathode pellets. Then, the cathode pellet was connected to a stainless-steel wire to assemble the cathode. A high-density graphite rod (Ø 10 × 60 mm) served as the anode. A eutectic mixture of $CaCl_2$-NaCl (Tianjin Kemiou Chemical Reagent Co., Ltd., China, Analytical reagent) was used as the electrolyte, which was packed in an alumina crucible and dehydrated at 300 °C for 24 h.

The alumina crucible, filled with the mixed salt, was introduced into the bottom of a stainless-steel reaction vessel. Then, the vessel was sealed and ultra-high-purity argon gas was flushed into the reactor to provide a protective atmosphere. The furnace temperature was increased to 850 °C under continuous argon circulation. The pre-electrolysis was performed at 2.5 V for 2 h using two graphite rods as anode and cathode to remove any electrochemically active impurities from the melt. Then, a fresh graphite rod and cathode were lowered into the melt. The electrolysis was carried out at 3.1 V. After electrolysis, the samples were carefully rinsed with distilled water several times to remove the adhering salt and immersed in distilled water for 24 h, followed by drying at 80 °C.

The phase composition was identified by using X-ray diffraction (XRD, Rigaku D/Max-2500PC). The morphology and chemical composition were determined by a field-emission scanning electron microscope (FESEM, Carl Zeiss-EVO18), coupled with energy-dispersive X-ray spectroscopy (EDX), and transmission electron microscope (TEM, JEM-1200F).

3. RESULTS AND DISCUSSION

$ZrSiO_4$, Fe_2O_3 and carbon black powders were mixed in a molar ratio of 1:0.5:2.5. Then, the mixture was compacted and sintered under Ar flow at 950 °C for 4 h. As shown in Fig. 1a, $ZrSiO_4$ and Fe_2O_3 phases were present in $ZrSiO_4/Fe_2O_3/C$ (1:0.5:2.5) mixed pellets before sintering. However, the diffraction peaks of carbon were not observed due to the amorphous structure of carbon black. Moreover, Fe_2O_3 was completely converted into Fe after sintering, as shown in Fig. 1b. Hence, the cathode pellet rendered higher electrical conductivity than the starting material. These results indicate that the chemical reaction occurred between Fe_2O_3 and carbon during sintering via Reaction (1). Therefore, the sintered pellet consisted of $ZrSiO_4$, Fe, and C in the molar ratio of 1:1:1.

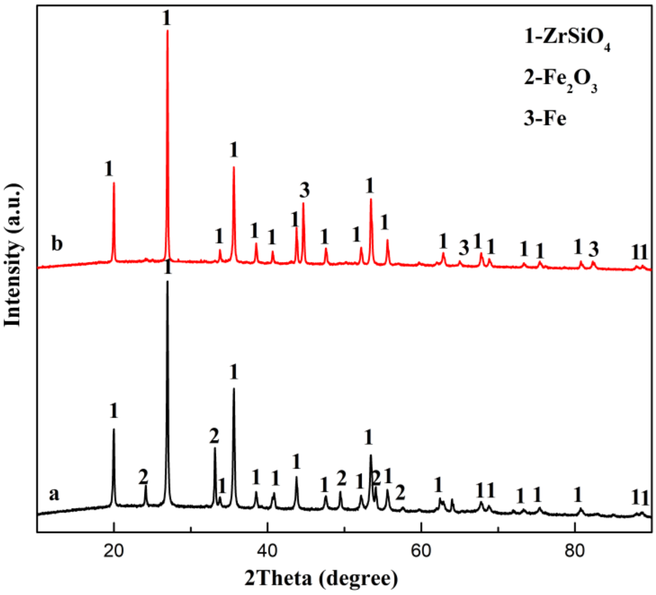

Figure 1. XRD patterns of $ZrSiO_4/Fe_2O_3/C$ (1:0.5:2.5) mixed pellets (a) before and (b) after sintering.

Fig. 2a presents the morphology of as-sintered pellet, showing micron-sized block-shaped particles, surrounded by carbon nanoparticles. The combination of EDS (Fig. 2b) and XRD (Fig. 1b) results revealed that the micron-sized particles are $ZrSiO_4$ and Fe. In addition, the porous structure of sintered pellet can be ascribed to the gas emission during sintering, which facilitates the mass transfer during the electrolysis process.

$$Fe_2O_{3(s)} + 3C_{(s)} = 2Fe_{(s)} + 3CO_{(g)} \qquad \Delta G^{\theta}_{T=1223K} = -155.75\,kJ \cdot mol^{-1} \qquad (1)$$

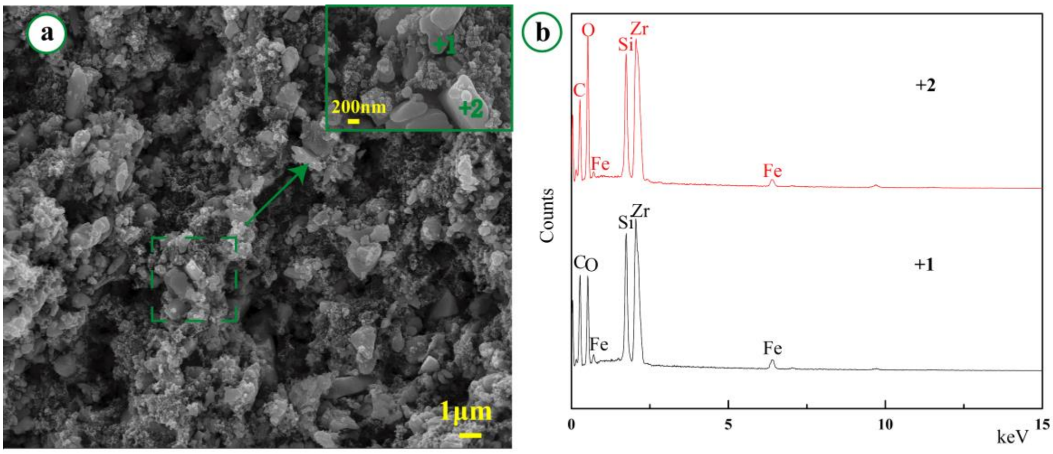

Figure 2. (a) SEM image of $ZrSiO_4/Fe_2O_3/C$ mixed pellet after sintering at 950 °C for 4 h, where the inset shows the partially-enlarged part from (a), and (b) EDS spectra from point 1 and 2 (panel a).

The $ZrSiO_4/Fe/C$ (1:1:1) cathode pellets were electrolyzed under 3.1 V at 850 °C for different times. Fig. 3a presents the XRD pattern of cathode pellet after electrolysis for 0.5 h, showing the presence of $CaZrO_3$, $Ca_xZr_{1-x}O_x$ (CSZ), Fe_3Si and Fe_5Si_3 phases. The low-intensity diffraction peaks can be indexed to Ca_2SiO_4 and Fe phases, whereas the remaining XRD peaks correspond to ZrC, which are shifted towards the higher diffraction angles. Hence, the lattice parameters of carbide phase are obviously smaller than the stoichiometric ZrC, as shown in Fig. 4a, which is generally attributed to the presence of oxygen and formation of oxycarbide phase ($ZrC_\alpha O_{1-\alpha}$). The existence of $CaZrO_3$, CSZ and Ca_2SiO_4 phases indicates that $ZrSiO_4$ is decomposed into calcium-containing intermediate compounds in the presence of CaO. The possible cathodic reactions are described in Eq. (2)[26] and (3). One should note that the CaO was introduced due to the combination of electrochemically-generated O^{2-} and Ca^{2+} ions from the melt or thermal drying of calcium chloride[27-29]. Meanwhile, the electro-deoxidation of the cathode has occurred, which can be confirmed by the appearance of Fe_3Si, Fe_5Si_3 and $ZrC_\alpha O_{1-\alpha}$ phases. This result suggests that $Ca_xZr_{1-x}O_x$ and $CaZrO_3$ are reduced to $ZrC_\alpha O_{1-\alpha}$ in the presence of carbon, as shown by Eq. (4) and (5)[30], respectively. Also, Ca_2SiO_4 is reduced to Si (Eq. 6)[26], followed by the removal of oxygen-ions from the cathode. Then, Fe and Si react to form Fe_3Si and Fe_5Si_3, according to Eq. (7) and (8), respectively. XRD patterns exhibit that the intensity of diffraction peaks, corresponding to the $ZrC_\alpha O_{1-\alpha}$ phase, increased with increasing electrolysis time and the peaks gradually shifted to lower diffraction angles. Hence, the cell parameters of $ZrC_\alpha O_{1-\alpha}$ phase progressively increased, as shown in Fig. 4, indicating that the oxygen content in $ZrC_\alpha O_{1-\alpha}$ phase decreased with increasing electrochemical reduction time. Finally, ZrC is formed according to Eq. (9)[30]. In addition, the formation of Fe-Si intermetallics follows the given sequence during electrolysis (Fe_3Si→Fe_5Si_3→FeSi), which is in good agreement with the thermodynamic analysis of the corresponding reactions, as shown in Table 1. With the increase of Fe content in the cathode, both FeSi and Fe phases have been detected in the XRD pattern of $ZrSiO_4$/Fe/C (1:1.5:1) pellet after electrolysis for 20 h, as shown in Fig. 3d. Correspondingly, the iron-containing metal phase is composed of FeSi and Fe. It can be concluded that the composition of iron-based metallic phase in the final product can be controlled by adjusting Fe content in cathode, which is determined by the amount of Fe_2O_3 in the cathode precursor. The overall cathodic reactions are more complicated than the presented steps. The reaction steps may occur dynamically and overlap during the electrolysis process. Furthermore, it has been reported that the ZrC-reinforced iron-based composites can be synthesized by aluminothermic reduction of Fe_2O_3 and $ZrSiO_4$ in the presence of carbon[12]. However, it has been found that, along with ZrC, other phases (Fe_3Al, $FeZr_4$) were inevitably formed. Therefore, in the current work, the Zr recovery in the form of ZrC and product purity is much higher than the aluminothermic reaction. Also, the composition of the as-prepared product can be more easily controlled by the proposed method.

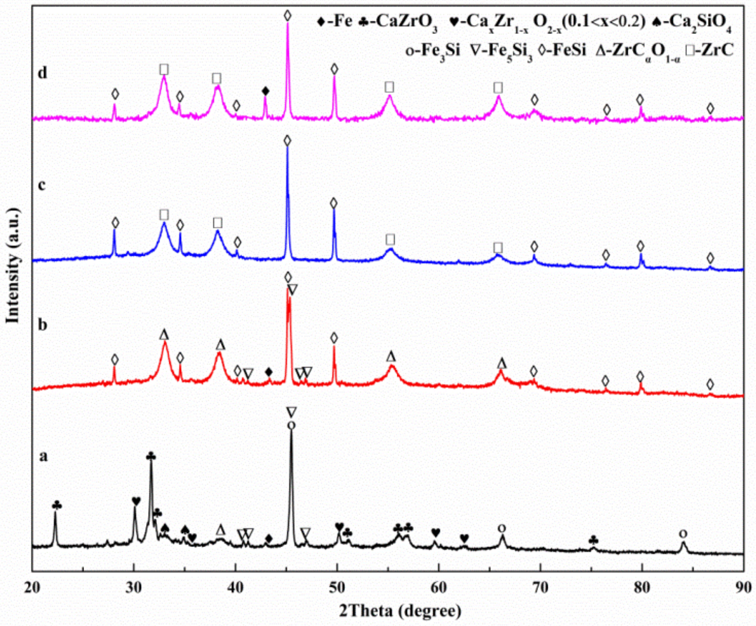

Figure 3. XRD patterns of $ZrSiO_4$/Fe/C(1:1:1) cathode pellets after electrolysis at 3.1 V for (a) 0.5 h, (b) 10 h and (c) 20 h, and (d) $ZrSiO_4$/Fe/C(1:1.5:1) cathode pellet after electrolysis at 3.1 V for 20 h.

$$(1\text{-}x)\,ZrSiO_4+(2\text{-}x)\,Ca^{2+}+(2\text{-}x)\,O^{2-}=Ca_xZr_{1\text{-}x}O_{2\text{-}x}+(1\text{-}x)Ca_2SiO_4 \tag{2}$$

$$ZrSiO_4+3Ca^{2+}+3O^{2-}=CaZrO_3+Ca_2SiO_4 \tag{3}$$

$$Ca_xZr_{1\text{-}x}O_{2\text{-}x}+2(1\text{-}x)(1+\alpha)e+\alpha(1\text{-}x)C=(1\text{-}x)\,ZrC_\alpha O_{1\text{-}\alpha}+xCaO+(1\text{-}x)(1+\alpha)O^{2-} \tag{4}$$

$$CaZrO_3+2(1+\alpha)e+\alpha C=ZrC_\alpha O_{1\text{-}\alpha}+CaO+(1+\alpha)O^{2-} \tag{5}$$

$$Ca_2SiO_4 + 4e = Si + 2CaO + 2O^{2-} \quad (6)$$

$$3Fe + Si = Fe_3Si \quad (7)$$

$$5/3Fe + Si = 1/3Fe_5Si_3 \quad (8)$$

$$ZrC_{\alpha}O_{1-\alpha} + 2(1-\alpha)e + (1-\alpha)C = ZrC + (1-\alpha)O^{2-} \quad (9)$$

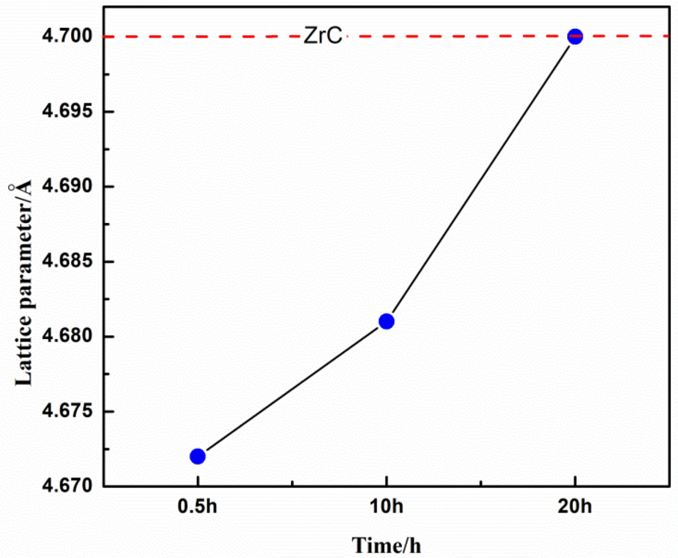

Figure 4. The change in lattice parameter of $ZrC_{\alpha}O_{1-\alpha}$ phase with electrolysis time.

Table 1. The change in standard Gibbs free energy of different reactions at 850 °C

Reaction	ΔG^{θ}(kJ·mol^{-1})
$3Fe + Si = Fe_3Si$	-101
$5/3Fe + Si = 1/3Fe_5Si_3$	-87
$Fe + Si = FeSi$	-75
$5/4Fe_3Si + Si = 3/4Fe_5Si_3$	-70
$1/2Fe_3Si + Si = 3/2FeSi$	-61
$1/2Fe_5Si_3 + Si = 5/2FeSi$	-60

Fig. 5a shows the cross-sectional SEM image of $ZrSiO_4$/Fe/C (1:1:1) pellet after electrolysis at 3.1 V for 0.5 h. The morphology of the inner layer is shown in Fig. 5b. It can be seen that coarse and bumpy particles are located between fine particles. The XRD (Fig. 3a) and EDS (Fig. 5d) analysis revealed that the above mentioned coarse and bumpy particles are calcium-containing intermediate compounds, such as $CaZrO_3$, $Ca_xZr_{1-x}O_x$ and Ca_2SiO_4. Moreover, the small holes on the surface of particles may result from the release of CaO and O^{2-} during electrolysis. The surface layer of the pellet, electrolyze at 3.1 V for 0.5 h, is composed of interconnected nanoparticles (Fig. 5c). One should note that the large micron-sized particles, consisting of $ZrSiO_4$ and Fe, have been vanished after electrolysis for 0.5 h, which can be attributed to the rearrangement of atoms and ions in the lattice due to the decomposition of $ZrSiO_4$, removal of oxygen, carbonization and alloying reactions. The XRD (Fig. 3a) and EDS (Fig. 5d) results revealed that the surface layer primarily consists of Fe-Si intermetallic and $ZrC_{\alpha}O_{1-\alpha}$. In addition, the electro-deoxidation of the cathode pellet proceeded from the surface to interior. As shown in Fig. 5e, after 20 h of electro-reduction, the fully-reduced sample consists of homogeneous nanoparticles, showing excellent sinterability due to the metallic nature of FeSi phase. Fig. 5f presents the TEM image of $ZrSiO_4$/Fe/C (1:1:1) pellet after electrolysis at 3.1 V for 20 h. It can be seen that the ZrC particles (<20 nm) are uniformly dispersed within the FeSi matrix.

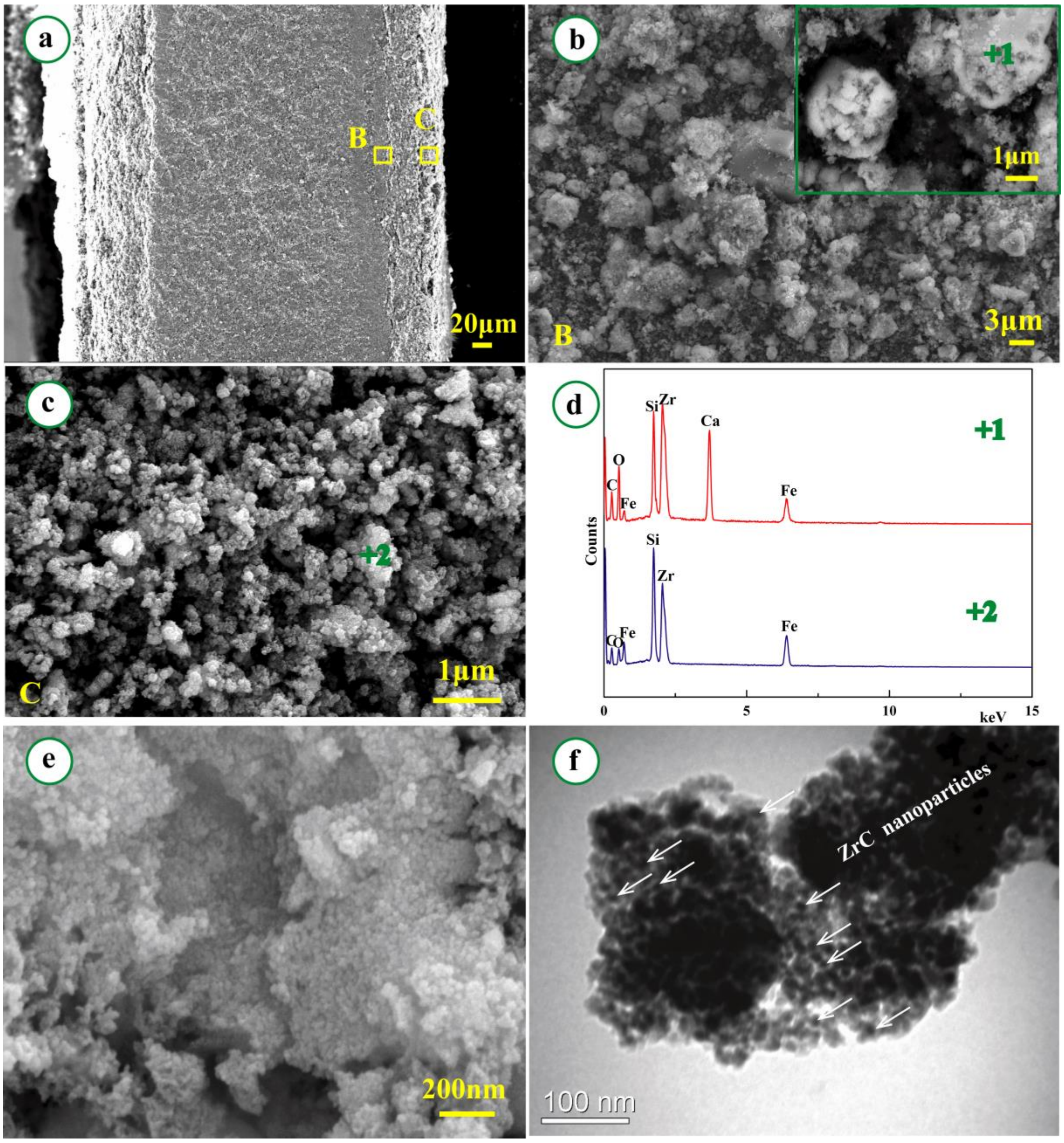

Figure 5. SEM images of $ZrSiO_4$/Fe/C (1:1:1) pellet after electrolysis at 3.1 V for 0.5 h: (a) cross-sectional SEM image, (b) Area-B, where the inset shows the partially-enlarged image of panel (b), and (c) the high-magnification SEM image of Area-C; (d) EDS spectra from Point-1 (panel b) and Point-2 (panel c); (e) SEM and (f) TEM images of $ZrSiO_4$/Fe/C (1:1:1) pellet after electrolysis at 3.1 V for 20 h.

Based on the above discussion, the pathway of molten salt electrosynthesis of FeSi-ZrC composite from the mixture of $ZrSiO_4$/Fe_2O_3/carbon is schematically proposed in Fig. 6. First, Fe_2O_3 is reduced to Fe due to the presence of carbon during sintering. Then, $ZrSiO_4$ is decomposed into intermediate phases, such as $CaZrO_3$ (or $Ca_xZr_{1-x}O_{2-x}$) and Ca_2SiO_4, through the participation of CaO in the melt. Meanwhile, the tetravalent zirconium compounds are electro-deoxidized in the presence of carbon to form ZrC_xO_{1-x}. Moreover, Ca_2SiO_4 is electro-reduced to Si, which combines with Fe to form Fe_3Si and Fe_5Si_3. Finally, the ZrC_xO_{1-x} phase is gradually reduced to ZrC and Fe-Si intermetallics are gradually transformed into FeSi according to the given sequence: $Fe_3Si \rightarrow Fe_5Si_3 \rightarrow FeSi$.

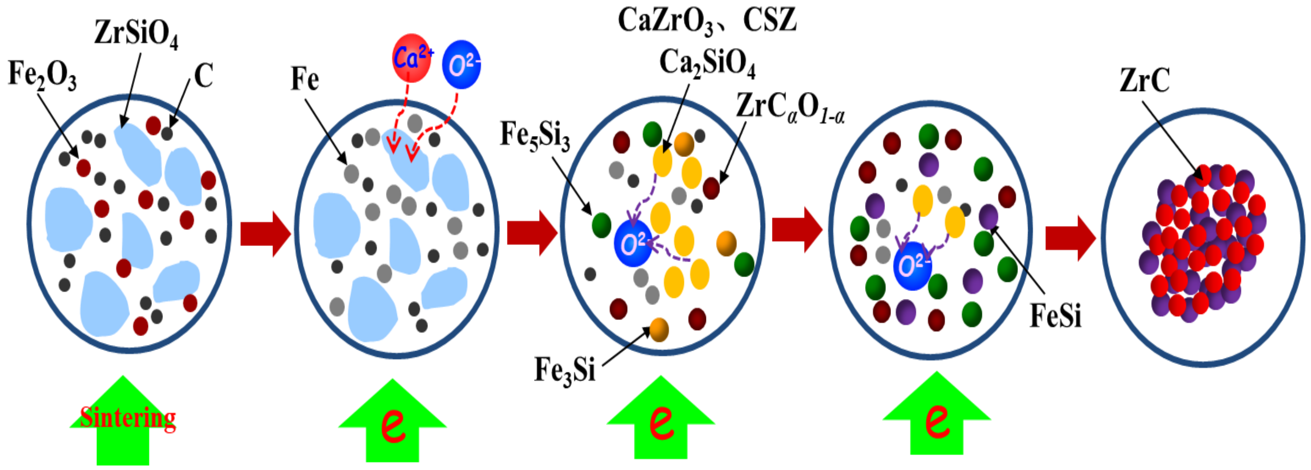

Figure 6. Schematic illustration of the FeSi-ZrC composite formation by the electrochemical reduction process.

4. CONCLUSIONS

In summary, nano-sized iron-based ZrC composite powder has been successfully synthesized by a one-pot electrolytic process using low-cost $ZrSiO_4$, Fe_2O_3 and carbon precursors in $CaCl_2$-NaCl molten salt under 3.1 V at 850 °C. It has been found that the composition of Fe-based metallic phases can be controlled by adjusting the amount of Fe_2O_3 in the precursor. The mixture of $ZrSiO_4$, Fe_2O_3 and carbon has been converted into FeSi-ZrC composite in three steps. First, the carbothermal reduction of Fe_2O_3 resulted in the formation of Fe during sintering. Second, $ZrSiO_4$ has been decomposed into calcium-containing intermediate compounds, such as $CaZrO_3$, $Ca_xZr_{1-x}O_x$ and Ca_2SiO_4, in the presence of CaO. Meanwhile, the tetravalent zirconium intermediate compounds have been reduced to the oxycarbide phase, i.e., $ZrC_\alpha O_{1-\alpha}$, due to the synergistic influence of electro-deoxidation and carbonization. Moreover, Ca_2SiO_4 has been electrochemically reduced into Si, which subsequently reacted with Fe to form Fe_3Si and Fe_5Si_3. Third, the ZrC_xO_{1-x} phase has been gradually reduced into ZrC due to oxygen removal and FeSi has been formed according to the given sequence: $Fe_3Si \rightarrow$

Fe_5Si_3→ FeSi. The current work presents an easy and direct electrochemical synthesis route to convert $ZrSiO_4/Fe_2O_3/C$ precursor into iron-based ZrC composites.

ACKNOWLEDGEMENTS

This work was financially supported by the Higher Educational Scientific Research Projects of Inner Mongolia Autonomous Region (Grant No. NJZZ19066), Natural Science Foundation of Inner Mongolia Autonomous Region (Grant No. 2019MS05066), and Science and Technology Major Project of Inner Mongolia Autonomous Region (Grant No. 2018-810).

References

1. E. Pagounis, M. Talvitie and V.K. Lindroos, *Metall. Mater. Trans. A,* 27A (1996) 4171.
2. B.S. Terry and O.S. Chinyamakobvu, *Mater. Sci. Technol.,* 7 (1991) 842.
3. C. Raghunath, M.S. Bhat and P.K. Rohatgi, *Scr. Metall. Mater.,* 32 (1995) 577.
4. Y. Chen, *Scr. Mater.,* 36 (1997) 989.
5. L. Wang, F. Zhang, W. Dai, Q. Cheng, K. Zhang, Y. Wu, Y. Xiong, Y. Lu, Q. Wu and X. He, *Chem. Lett.,* 48 (2019) 604.
6. K. Li, X. Zhou, Z. Zhao, C. Chen, C. Wang, B. Ren and L. Zhang, *J. Solid State Chem.,* 258 (2018) 383.
7. M. Mahdavi, M. Ramazani and Z. Darvishi, *Adv. Powder Technol,* 27 (2016) 1547.
8. Y u. L. Krutskii, E. A. Maksimovskii, M. V. Popov, O. V. Netskina, N. Yu. Cherkasova, T. S. Kvashina, V. I. Chushenkov, A. I. Smirnov, A. V. Felof'yanova and A. I. Aparnev, *Russ. J. Appl. Chem.,* 91(3) (2018) 428.
9. Q. Zhang, J. He, W. Liu and M. Zhong, *Surf. Coat. Technol.,* 162 (2003) 140.
10. M. Jiang, K. Oikawa, T. Lkeshoji, L. Wulff and K. Ishida, *J. Phase Equilib.,* 22 (2001) 406.
11. T.K. Bandyopadhyay and K. Das, *J. Mater. Process. Technol.,* 178 (2006) 335.
12. K. Das and T.K. Bandyopadhyay, *Mater. Sci. Eng., A,* 379 (2004) 83.
13. G. Zhang and D. Gu, *Appl. Surf. Sci.,* 273 (2013) 364.
14. K. Das, T.K. Bandyopadhyay and S. Das, *J. Mater. Sci.,* 37 (2002) 3881.
15. E. Pagounis, M. Talvitie and V.K. Lindroos, *Powder Metall.,* 40(1) (1997) 55.
16. A.A. Popov and M.M. Gasik, *Scr. Mater.,* 35(5) (1996) 629.
17. Q. Fan, H. Chai and Z. Jin, *J. Mater. Process. Technol.,* 96 (1999) 102.
18. G.Z. Chen, D.J. Fray and T.W. Farthing, *Nature,* 407 (2000) 361.
19. J. Peng, H. Chen, X. Jin, T. Wang, D. Wang and G.Z. Chen, *Chem. Mater.,* 21 (2009) 5187.
20. W. Xiao, J. Zhou, L. Yu, D. Wang and X.W. Lou, *Angew. Chem. Int. Ed.,* 55 (2016) 1.
21. A.M. Abdelkader and D.J. Fray, *J. Eur. Ceram. Soc.,* 32 (2012) 4481.
22. X.Y. Yan, M.I. Pownceby, M.A. Cooksey and M.R. Lanyon, *Trans. Inst. Min Metall. C*, 118 (2009) 23.
23. Q.S. Song, Q. Xu, J.C. Meng, T.P. Lou, Z.Q. Ning, Y. Qi and K. Yu, *J. Alloys Compd.,* 647 (2015) 245.
24. X. Zou, X. Lu, Z. Zhou and C. Li, *Electrochem. Commun.,* 21 (2012) 9.
25. Q. Song, Q. Xu, L. Xu, Z. Ning, T. Lou, H. Xie, Y. Qi and K. Yu, *J. Alloys Compd.,* 690 (2017) 116.
26. H. Liu, Y. Cai, Q. Xu, Q. Song and H. Liu, *New J. Chem.***,** 39 (2015), 9969.
27. G.Z. Chen and D.J. Fray, *J. Electrochem. Soc.,* 149 (2002) E455.
28. C. Schwandt and D.J. Fray, *Electrochim. Acta,* 51 (2005) 66.

29. R.O. Suzuki, M. Aizawa and K. Ono, *J. Alloys Compd.*, 288 (1999) 173.
30. H. Liu, W. Song, Q. Xu, W. Ma and Y. Bai, *Int. J. Electrochem. Sci.*, 15 (2020) 6238.